




## Article

# Channel Impulse Response at 60 GHz and Impact of Electrical Parameters Properties on Ray Tracing Validations

Huthaifa Obeidat <sup>1,\*</sup>, Atta Ullah <sup>2</sup>, Ali AlAbdullah <sup>2</sup>, Waqas Manan <sup>2</sup>, Omar Obeidat <sup>3</sup>, Wafa Shauieb <sup>4</sup>, Yousef Dama <sup>5</sup>, Chakib Kara-Zaïtri <sup>2</sup> and Raed Abd-Alhameed <sup>2,6</sup>

<sup>1</sup> Faculty of Engineering, Jerash University, Jerash 26150, Jordan

<sup>2</sup> Faculty of Engineering and Informatics, University of Bradford, Bradford BD7 1DP, UK; a.ullah5@bradford.ac.uk (A.U.); a.a.abdUllah1@bradford.ac.uk (A.A.); waqas\_manan2000@yahoo.com (W.M.); C.Karazaitri@bradford.ac.uk (C.K.-Z.); r.a.a.abd@bradford.ac.uk (R.A.-A.)

<sup>3</sup> College of Engineering, Wayne State University, Detroit, MI 48202, USA; omar.obeidat@wayne.edu

<sup>4</sup> Faculty of Engineering, Omar Al-Mukhtar University, Al Bayda 00218-84, Libya; wafashuaieb@yahoo.com

<sup>5</sup> Faculty of Engineering and Information Technology, An-Najah National University, Nablus 44859, Palestine; yasdama@najah.edu

<sup>6</sup> Information and Communication Department, Basra University College of Science and Technology, Basra 61004, Iraq

\* Correspondence: h.obeidat@jpu.edu.jo

**Abstract:** This paper outlines a study of the effect of changing the electrical properties of materials when applied in the Wireless InSite (WI) ray-tracing software. The study was performed at 60 GHz in an indoor propagation environment and supported by Line of Sight (LoS) and Non-LoS measurements data. The study also investigates other factors that may affect the WI sensitivity, including antenna dimensions, antenna pattern, and accuracy of the environment design. In the experiment, single and double reflections from concrete walls and wooden doors are analysed. Experimental results were compared to those obtained from simulation using the WI. It was found that materials selected from the literature should be similar to those of the environment under study in order to have accurate results. WI was found to have an acceptable performance provided certain conditions are met.

**Keywords:** mm-wave propagation; indoor propagation; channel measurements; ray tracing



**Citation:** Obeidat, H.; Ullah, A.; AlAbdullah, A.; Manan, W.; Obeidat, O.; Shauieb, W.; Dama, Y.; Kara-Zaïtri, C.; Abd-Alhameed, R. Channel Impulse Response at 60 GHz and Impact of Electrical Parameters Properties on Ray Tracing Validations. *Electronics* **2021**, *10*, 393. <https://doi.org/10.3390/electronics10040393>

Academic Editors: Giovanni Leone and Athanasios Kanatas

Received: 5 December 2020

Accepted: 28 January 2021

Published: 5 February 2021

**Publisher's Note:** MDPI stays neutral with regard to jurisdictional claims in published maps and institutional affiliations.



**Copyright:** © 2021 by the authors. Licensee MDPI, Basel, Switzerland. This article is an open access article distributed under the terms and conditions of the Creative Commons Attribution (CC BY) license (<https://creativecommons.org/licenses/by/4.0/>).

## 1. Introduction

With recent development in manufacturing front-end devices, it is now possible to utilise high frequencies in communications, including the 60 GHz band [1] which is suitable for 5G systems [2]. The use of high-frequency bands in communication systems is advantageous as it allows for higher bandwidths and hence higher data rates. Since the coverage area is small, frequency reuse is widely applicable. Moreover, using higher frequencies allows a smaller size of radio frequency RF components. This saves more space and therefore supports the use of antenna arrays—an essential feature for beamforming (BF) techniques which yield higher density cells and a higher throughput [3,4]. Unlike WLAN systems, interference is not a concern. However, the manufacturing process is more complicated [5].

At millimetre frequencies, the free space propagation losses (FSPL) is larger compared to those at lower frequencies. For example, over a 5 km distance, FSPL at 60 GHz is 35.6 dB more than at 1 GHz [6]. Moreover, wall penetration losses are larger since conductivity increases with frequency. Moreover, the effect of reflection and scattering becomes more apparent because object sizes become comparable to the wavelength [7]. Moreover, the atmospheric attenuation caused by oxygen and water drops adds more to the path loss especially at 60 GHz [7]. Due to the aforementioned causes and the small antenna aperture at this band, highly directional antennas with large arrays are used [3]. Additionally, since

the total noise power for wider bandwidth is higher, 60 GHz systems operate a 10 dB higher power compared to the IEEE 802.11n systems, where the local mean of power reduces the fast fading effect [8].

Different countries have different frequency allocations for the 60 GHz band. In the USA and Canada, the allocated band is within 57–64 GHz, while the EU, Japan and China have bands within 57–66 GHz, 59–66 GHz and 59–66 GHz respectively.

The data rate can reach up to 6.7 Gbps using directional antennas [9] within indoor environments. IEEE 802.11 ay standard has been issued as a follow-up to IEEE 802.11 ad, with the aim of having data rate in the range 20–40 Gbps [10,11]. The available 60 GHz band has 14 GHz bandwidth approximately, and this can be divided into 2.16, 4.32, 6.48 and 8.64 GHz channels [12]. High order modulation schemes with channel bonding are used to extend the available bandwidth [10], for example, a data rate of 42.24 Gbps can be achieved using a 4-channel bonding (each channel with 2.16 GHz) with 0.04 m distance, 64 quadrature amplitude modulation (QAM) and 169 mW consumed power at transmission mode and 139 mW at reception mode [10]. The 60 GHz band propagation has been investigated for indoor environments [13–16], outdoor environments [16–18] and outdoor to indoor environments [19,20].

In the non-line-of-sight (NLOS) propagation, the effect of building materials is more evident. Many studies investigated their effect on propagation by identifying the relative permittivity and conductivity of these materials, for mm-wave frequencies, permittivity tends to increase unnoticeably with frequency, however; conductivity tends to increase remarkably [21]. In this study, two materials have been investigated: namely concrete and wood.

Wireless InSite Ray-tracer is a commercial software used to predict channel parameters within indoor and outdoor environments. The software has been validated at 900 MHz and 1800 MHz [22] and at 2.4 GHz and 5 GHz [23,24]. Wireless InSite considers the effects of material electrical properties. It also allows the user to configure waveform, antenna types and the properties of the transmitter and receivers. In this scenario, a sinusoidal waveform is used for simulation at 60 GHz [25]. This paper aims to investigate the accuracy of the results when applying different electrical properties of concrete and wood in Wireless InSite. This paper is divided into four main sections, including the design of the channel sounder, an explanation of the experimental setup, a discussion of the results obtained, and finally concluding remarks.

## 2. Channel Sounder

A channel sounder is usually used to measure channel impulse response  $h(\tau)$  or its frequency response  $H(f)$  in the frequency domain. Since the channel is dependent on frequency, time and position, a channel can be identified by the delay spread, the angle of arrival/departure, the Doppler shift and the signal strength received. Figures 1 and 2 show the architecture of the channel sounder.

The message signal is implemented using the Altera FPGA board (Figure 2d) which is programmed to provide a pseudo-random binary sequence of  $2^m-1$  sequence, where  $m$  ranges from 6 to 10. A CO2201A converter evaluation board (Figure 2b) controls the transmitter Tx and receiver Rx converter modules. The system developed has power detectors, a power amplifier, automatic gain control and a USB interface to control the modules. The Keysight digital storage oscilloscope (DSO) X-3014A (Figure 2a) has four channels. Each channel has a 200 MHz Bandwidth, which is equivalent to 400 MHz bandwidth ( $\pm 200$  MHz). Both the CO2201A and the DSO are connected to a PC via a USB, which generates commands. The sounder can readily be integrated with MATLAB, thus providing another facility for generating commands. Table 1 illustrates the channel sounder characteristics.

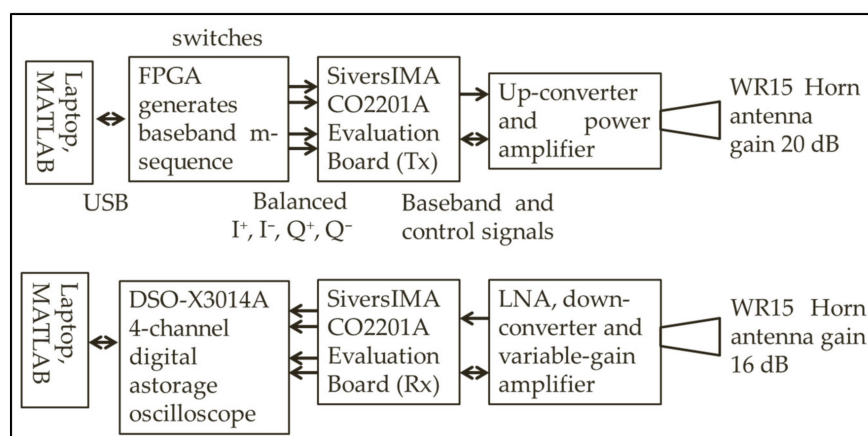
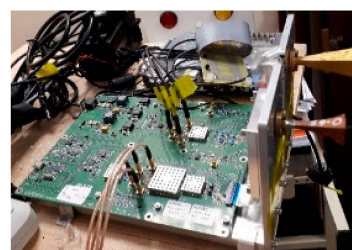


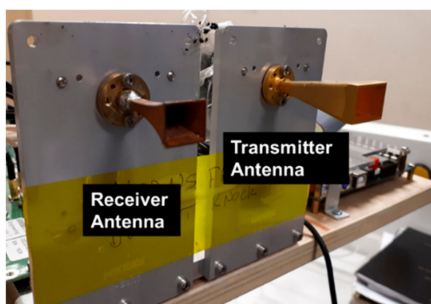
Figure 1. Channel Sounder architecture.



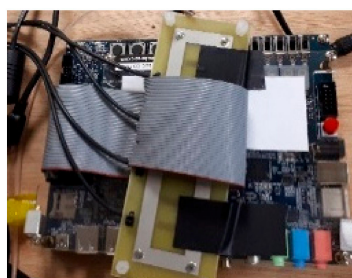
(a)



(b)



(c)



(d)

Figure 2. Channel sounder: (a) Keysight's DSO, (b) COST2201A evaluation board, (c) evaluation board antenna, (d) Altera FPGA board.

Table 1. Channel Sounder characteristics.

Item	Value
Internal pulse amplitude	5 V peak
Bit period	4 ns
Bandwidth of operation	400 MHz
EIRP *	32 dBm
Data rate	250 bps
sampling interval	2 ns
Sweep speed	10 $\mu$ s/div
HPBW * E (dB)	18.72°
HPBW H (dB)	23.03°

\* where EIRP is the effective isotropic radiated power and HPBW is the half-power beamwidth.

### 3. Experimental Setup

The 60 GHz band channel sounder can be used for two types of measurements: back-to-back measurements and radar measurements (Figure 3). In order to compensate for the non-ideal hardware transfer functions of the transmitter and receiver chains, system calibration is necessary.

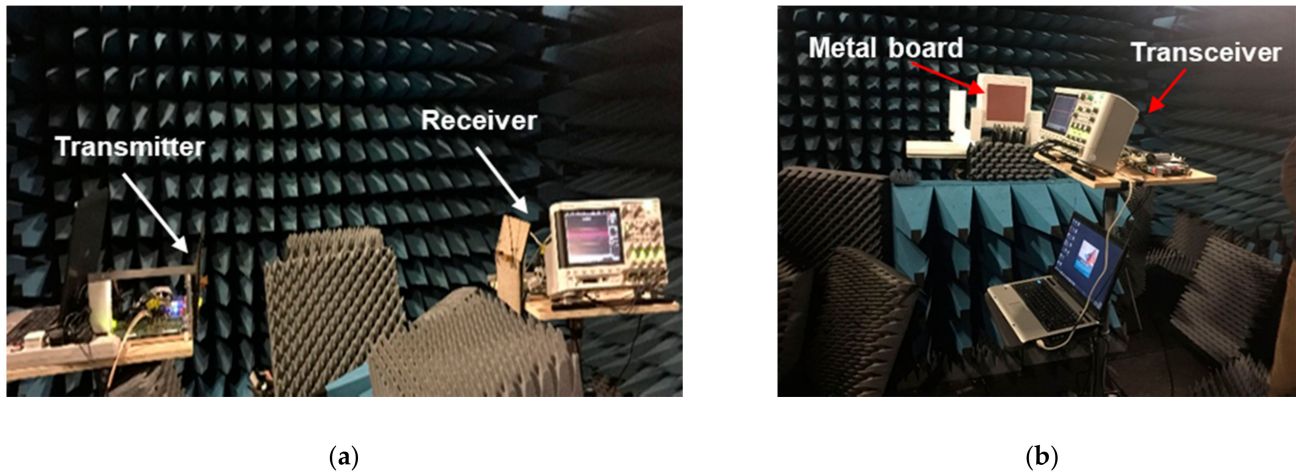


**Figure 3.** Calibration in the anechoic chamber, (a) back-back mode and (b) radar mode.

Calibration aims to reduce any measurement uncertainty by ensuring the accuracy of the test equipment. Calibration measures and controls uncertainties within measurement processes to an acceptable level. The anechoic chamber is used to provide a controlled environment, with a minimized electromagnetic interference, and walls of the chamber are covered with radio-frequency absorbers [26].

The COST2201A evaluation board has two sections as seen in Figure 2c: transmitter section and receiver section. Therefore, the board can operate only the transmitter as in Figure 4b, also, it can operate only the receiver as in Figure 4c. And finally, it can operate both sections as a transceiver. The first two functions are used the back-back measurements. While the transceiver function is used in radar mode. Therefore, we need two types of calibrations.

In the radar mode, the transmitter and receiver are co-located on the same board, so the transmitter antenna will transmit waves while the reflected/scattered wave will be received by the receiver antenna. In the case of back-back measurements, the transmitter section mounted on the board will operate (Figure 4b), and only the receiver section mounted on the board will receive (Figure 4c).

Each type of measurement requires its own calibration (Figure 3). Since Radars have the transmitter and receiver co-located, the synchronization is easier, and the absolute delay can be measured and yield the distance. In the calibration process, the distance between the transmitter and the receiver is 1 m. This distance ensures that the radiation pattern is in the far-field. Measurements over the whole frequency range of the sounder with 250 MHz steps were taken in radar mode. The distance between the antenna horn and the flat metal board is 0.5 m. Given that the wave will move forward and backwards, the total distance is 1 m. The calibration was performed in an anechoic chamber at the University of Bradford. The radar calibration setup includes reflections from a flat reflector and corner reflectors, it's worth mentioning that the size of the metal board has to be large enough to contain the first Fresnel zone of propagation.



(a)



(b)



(c)

**Figure 4.** 60 GHz Channel Sounder in Lab B3.26, (a) LOS scenario, (b) Transmitter, (c) Receiver.

The receiver and transmitter were synchronised, the synchronization is easier at radar mode since we used single evaluation board. However, while using two boards at back-back mode, both boards have to be synchronised. This can be achieved by controlling the two boards from one of them by giving the order through MATLAB.

Validation of Wireless InSite was performed in two indoor scenarios, LOS and NLOS. Both scenarios are conducted at the University of Bradford. The simulated environment took into account the fine details of the building for accurate validation. For all cases, the transmitted power was set to 30 dBm, while the transmitter antenna gain was set to 18 dBi.

### 3.1. LOS Experiment

The first step of this validation is the direct LOS propagation which was conducted in a lab room. Both the transmitter and the receiver used vertically polarised pyramidal horn antenna. The devices were placed in the lab room in LOS at 1.5 m height and separated by 5 m as shown in Figure 4. (Receiver's antenna gain is 18 dBi).

### 3.2. NLOS Experiment

In the NLOS scenario, measurements were conducted at three positions distributed in the lab area while rotating the receiver clockwise about the Z-axis (assuming the floor is on the  $xy$  plane). The same instruments used in the LOS experiment, are also used in the

NLOS experiment part. The transmitter was placed at the height of 2m, while the receiver was set to 1.5 m at all receiver points, as shown in Figure 5.



**Figure 5.** NLOS experiment at receiver position 1.

Material's electrical properties effect

Material dependence on operating frequency plays a major role in determining the radio coverage. The attenuation rate  $A$  (dB/m) is a function of conductivity  $\sigma$  and relative permittivity  $\epsilon_r$  [27]:

$$A = \begin{cases} 1636 \frac{\sigma}{\sqrt{\epsilon_r}} & \text{Dielectric} \\ 545.8 \sqrt{\sigma f_{\text{GHz}}} & \text{Conductor} \end{cases} \quad (1)$$

Both  $\epsilon_r$  and  $\sigma$  are frequency-dependent as shown as:

$$\epsilon_r = \alpha f_{\text{GHz}}^\beta \quad (2)$$

$$\sigma = \gamma f_{\text{GHz}}^\delta \quad (3)$$

where  $\alpha$ ,  $\beta$ ,  $\gamma$  and  $\delta$  are given by [27]. Many experimental studies have been conducted to find the values of  $\epsilon_r$  and  $\sigma$ . It was noted for the same type of material the values tend to vary, for example at 60 GHz, typical values of  $\epsilon_r$  and  $\sigma$  for aerated concrete are 2.26 and 0.3759 and for concrete are 6.14 and 1.0049 [28]. For plain wood,  $\epsilon_r$  and  $\sigma$  found to be 2.068 and 1.38 respectively at 60 GHz while for floor board  $\epsilon_r$  and  $\sigma$  are 3.91 and 1.1 respectively at the same frequency. For chipboard  $\epsilon_r$  and  $\sigma$  found to be 2.85 and 0.53 [29]. For structural bricks (i.e., with holes within),  $\epsilon_r$  and  $\sigma$  found to be 3.95 and 0.244 respectively at 60 GHz while paving bricks (without holes)  $\epsilon_r$  and  $\sigma$  found to be 3.26 and 0 for the same frequency.

Literature suggests that concrete complex permittivity changes with the type of concrete sample (i.e., aerated, lightweight or hardened) rather than changing the operating frequency for the same type of materials [30].

Complex permittivity of wood depends on the type of wood species, wood density, water content, temperature, the electric field orientation with respect to the grain, operating frequency and whether the wood experienced chemical treatment [30]. It was found that dielectric constant increases as temperature increases [31] while conductivity increases as water content increases [30]. Therefore chipboard, plywood, floorboard, Beechwood, Sipo and plain wood are expected to have different values for electrical constitutive parameters.

Typical values for relative permittivity and conductivity of concrete and wood from the literature at 60 GHz are presented in Table 2. These values will be used by Wireless InSite to predict the channel impulse response, which will be compared to the channel sounder results.

**Table 2.** Electrical constitutive parameters values for concrete and wood at 60 GHz.

Material	Reference	$\epsilon_r$	$\sigma$	Description
Concrete	[32] (a)	5.31	0.897	ITU-A
	[32] (b)	6.5	0.228	ITU-B
	[33]	7–13	-	Fares
	[34]	6.13	1.005	Fakharzadeh
	[35]	3.3	1.267	Lu
	[36] (a)	6.14	1.005	Correia-A
	[36] (b)	6.5	1.428	Correia-B
	[29]	11.47	0.988	Pinhasi
Wood	[32]	1.99	0.378	ITU
	[31]	2.1	0.2	Torgovnikov
	[34]	1.57	0.321	Fakharzadeh
	[37]	3.3	-	Affum
	[35]	2.8	0.001	Lu
	[36] (a)	1.57	0.321	Correia-A
	[36] (b)	1.54	0.118	Correia-B
	[38]	2.4	0.4	Salous
	[29] (a)	1.64	3.717	Pinhasi-A
	[29] (b)	2.068	1.38	Pinhasi-B

The software allows the user to set the number of paths. The more paths are considered, the more accurate the results, albeit with more processing time is required. Results show that having more than 10 paths does not improve the accuracy of the results. For this reason, the maximum number of paths was set to 10. Moreover, the maximum number of reflections and transmissions were set to 6 and 4 respectively. The Shoot and Bouncing Ray (SBR) was used as a ray-tracing method and the propagation method used was full 3D.

#### 4. Results and Discussion

Among the locations and rotations used, the receiver successfully received a signal from 18 receiver points. In the first position, measurements were observed successfully with rotations of 0°, 10°, 20° and 30°. In the second position, measurements were observed successfully with rotations of 120–180° and 210–250°. In the third position, only two rotations demonstrated reliable results; the simulated scenario was only for rotations 150° and 160°.

##### 4.1. LOS Scenario

The propagation paths for this scenario are presented Figure 6, where the loudest seven paths are shown; the colour of each path represents its strength as shown in the legend. The direct path is clearly the one with the strongest signal level.

The LOS scenario was conducted as in Figure 4a. Every effort was made to make the locations of Tx and Rx the same for both simulation and experimentation. The sounder was set up in such a way that it can be entirely controlled using MATLAB. This required the setup and control of the SiversIMA transceiver via the CO2201A evaluation board as well as control of the DSO-X3014A oscilloscope, which is used for data logging. The setup, control and measurements can automatically be carried out using a visa serial protocol over USB. In MATLAB, the operation frequency was chosen, then the calibration data to be applied (back-back mode or radar mode) was chosen, and the measured impulse response is calibrated. The output can be saved in a suitable MATLAB format, where the channel response can be extracted, including the time delay and the signal strength received. Figure 7 shows an example of the impulse response of the channel for the LOS measurements.

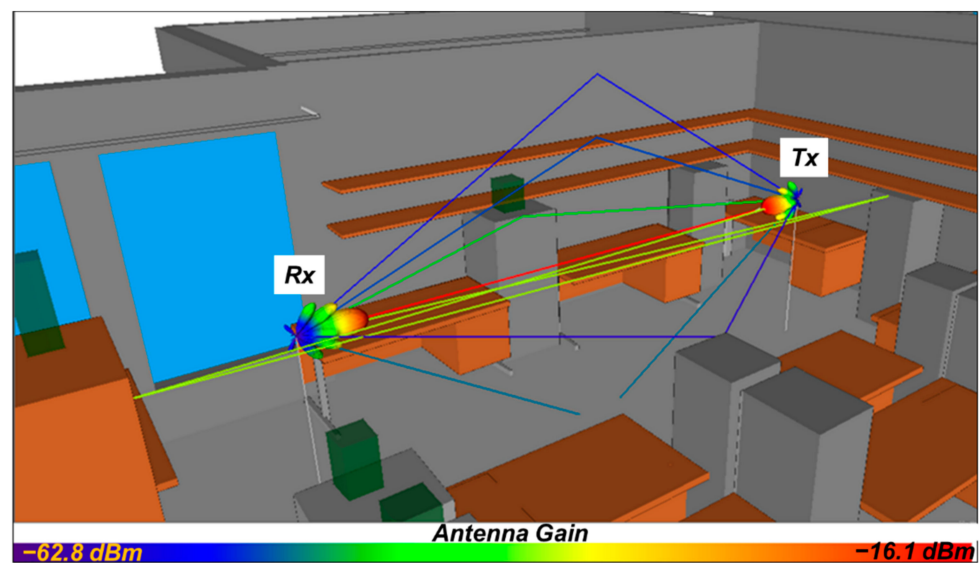


Figure 6. Strongest propagation paths for the LOS experiment.

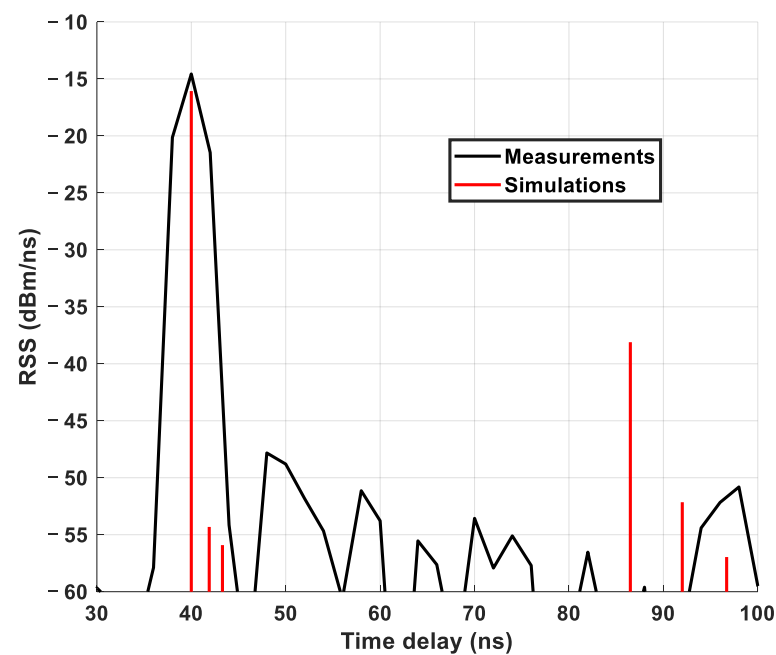


Figure 7. Comparison between simulations and measurements at LOS scenario.

Figure 7 shows a comparison between the simulation and measurements for the LOS scenario. Both results show good corroboration. For example, the direct path received power at  $-14.57$  dBm in the measurements, whilst  $-16.07$  dBm was recorded in the simulations.

#### 4.2. NLOS Scenario

##### 4.2.1. Position 1

For all rotations in Position 1, it was found that the strongest ray is reflected from one concrete wall as seen in Figure 8. This shows the propagation paths between the transmitter and receiver Rx1\_20° (receiver at the first position with 20° rotation). The colour of the Path represents the strength of the ray.

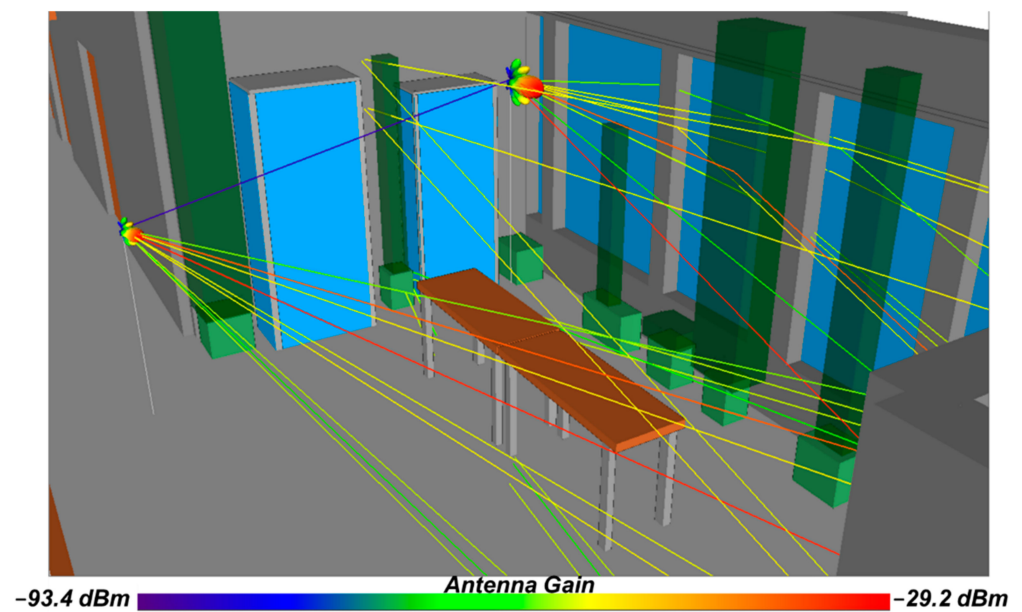


Figure 8. Reflection from the concrete wall (strongest path for all Rx1 points).

Figure 9 displays the power delay profile (PDP) at receiver Rx1\_20°, when the receiver antenna gain was set to 26 dB. The value of the concrete relative permittivity was 13 [33] and that for the conductivity was 0.8967 S/m [31]. The strongest ray arrived at 40 ns due to the reflection from the concrete wall as shown in Figure 8. Figure 9 shows good agreement between simulations and measurements. The received signal strength (RSS) was  $-23.91$  dBm in the measurements, while the simulated value was  $-25.63$  dBm. It can be seen in the same figure, that three simulated rays arrived at 40 ns, while the channel sounder has a wide peak, encompassing the convolved arrival paths, as it becomes difficult to distinguish between these incoming rays.

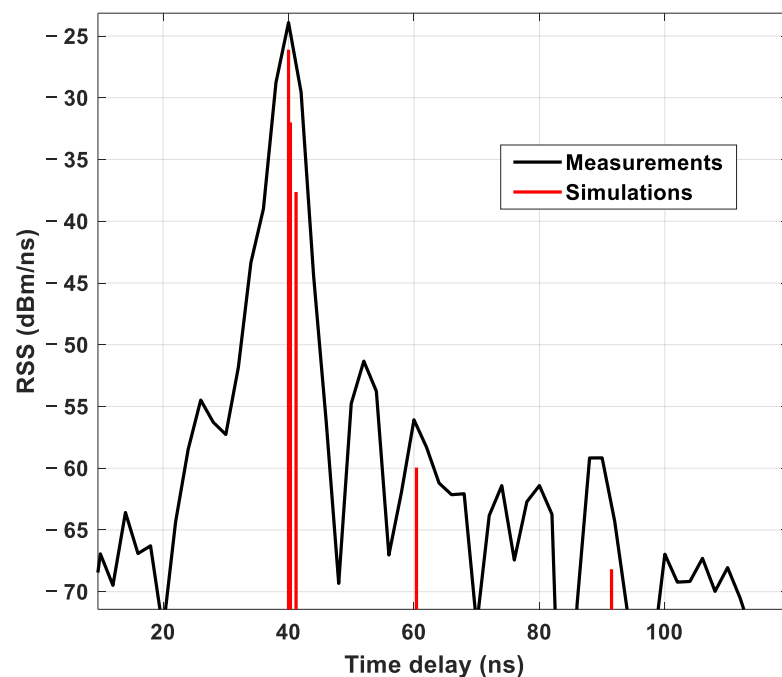


Figure 9. PDP at Rx1\_20°.

For any signal, the time resolution  $\Delta t$  and the spectral bandwidth  $\Delta f$  are related by:

$$\Delta t \times \Delta f \geq 1 \quad (4)$$

As seen in Equation (4), for a good time resolution ( $\Delta t$  is very small), the spectral BW should be large.

Figure 10 shows a performance comparison between measurements and simulated results at all Rx1 rotations, where various permittivity values, derived from the literature, are taken from Table 2. By using such values for concrete, simulated results appear to have up to 6 dB difference as indicated in the same figure. Having said this, the best-simulated results have a mean error of only around 2 dB when compared to those obtained from measurements.

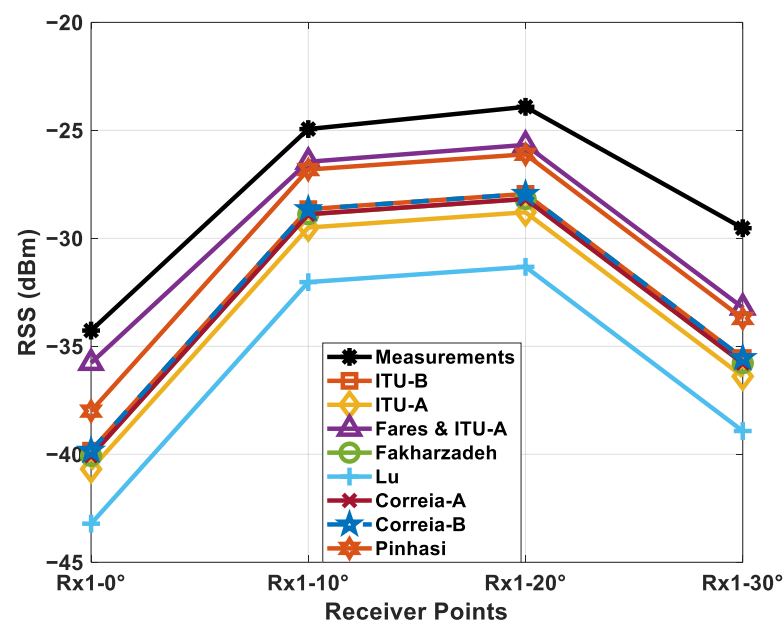


**Figure 10.** Performance comparison between measurements and data taken from references at Rx1.

Since it is very difficult to make the location/alignment of the transmitter and receiver exactly the same as in the measurements, despite careful practical preparations, the location of the receiver in the software was replaced within  $\pm 4$  cm in all dimensions and rotated  $\pm 2^\circ$ . Despite this, no significant difference was observed in the results.

#### 4.2.2. Position 2

In the second position, when the receiver was rotated with angles  $120^\circ$ – $180^\circ$ , the strongest ray was found to be in LOS with the transmitter, while for  $210^\circ$ – $250^\circ$  rotations, the strongest ray is reflected from a wooden board.

##### Case 1: LOS for ( $120^\circ$ – $180^\circ$ ) rotation

As seen in Figure 11, both Tx and Rx are in LOS while bore-sight for both antennae is not in direct contact. Since it is a LOS propagation, changing various permittivity values for building material will not affect the RSS of the strongest ray. Figure 11 shows the LOS and two reflected ray propagation paths from the transmitter to the receiver at the second position with a  $150^\circ$  rotation (receiver's antenna gain was set to 26 dB). The strongest path is the direct LOS between the transmitter and the receiver, whilst the second one is reflected from two concrete walls. From hereinafter, the display of propagation paths was limited to the strongest and most important path so the reader can follow the path more easily.

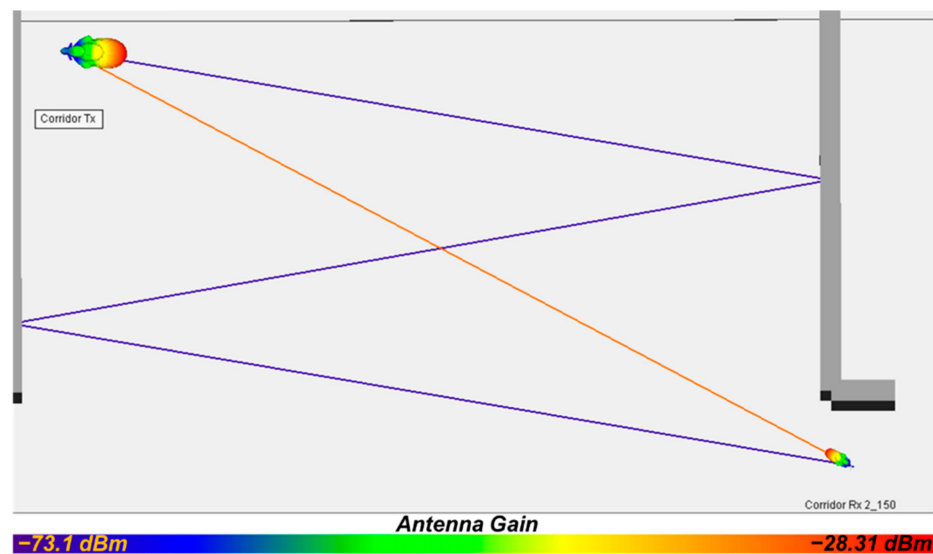


Figure 11. LOS and two reflected ray propagation paths from the transmitter to Rx2\_150°.

The power of these rays is shown diagrammatically in Figure 12. The RSS of the LOS measurement is  $-24.16$  dBm, while the simulated result is  $-28.31$  dBm. Table 3 presents a comparison between simulations and measurements at Rx2 ( $120$ – $180^\circ$ ) for the LOS component. As seen in the same table, the root mean square error (RMSE) is around  $8.64$  dB. It is worth mentioning that the receiver antenna sides are tilted to reduce the side lobes level. Such a feature is not available in WI, therefore, simulation results are expected to be slightly different from those in measurements, especially if both the transmitter and receiver are not in the boresight.

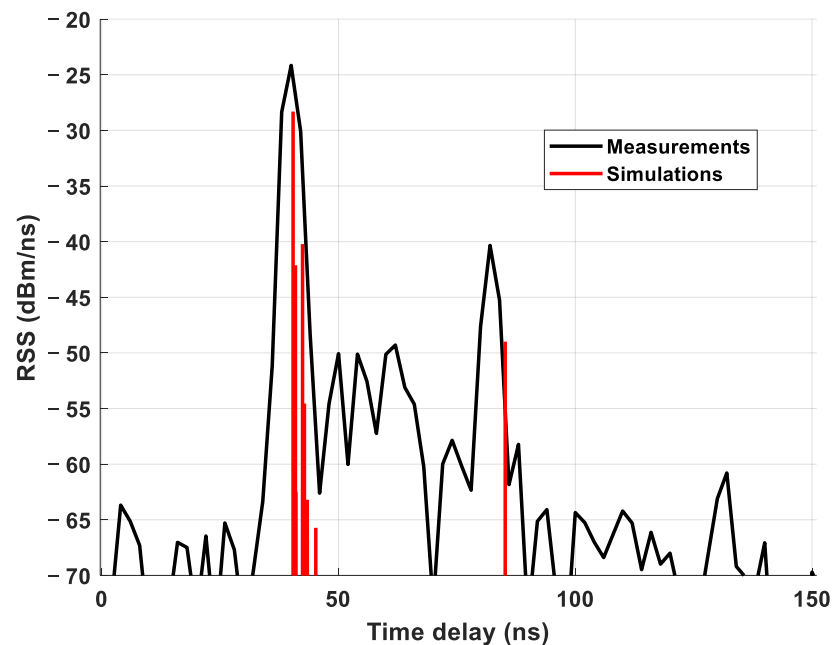


Figure 12. PDP at Rx2\_150°.

**Table 3.** Performance comparison between simulation and measurements at Rx2 (120–180°) for LOS component.

Receiver	Measured	Simulated
Rx2_120	−42.89	−51.742
Rx2_130	−33.82	−46.533
Rx2_140	−23.86	−34.464
Rx2_150	−24.16	−28.308
Rx2_160	−25.78	−30.812
Rx2_170	−52.46	−41.34
Rx2_180	−50.37	−48.37

The second ray reflected from two concrete walls, have a measured value of −40.34 dBm while the simulated value is −48.39 dB. Such a significant difference may be attributed to the effect of reflection from two concrete walls. It was found that the results are sensitive to changing the dimensions of the antenna. For example, adjusting the dimensions of the antenna around 1 cm can change the simulated results by more than 2 dB.

The results in the two reflections case shown in Table 4 demonstrate a similar behaviour to the single reflection case shown in Figure 10. The simulations that have the minimum average error with measurements in the two-reflection case have the closest RSS strength value to the measurements in the one reflection case. Moreover, the order of best and worst results did not change.

**Table 4.** Performance comparison between simulation and measurements at Rx2 (120–180°) for two walls reflection components.

Receiver	Measured	[33] + [32] (a)	[32] (a)	[32] (b)	[34]	[35]	[36] (a)	[36] (b)	[29]
Rx2_120	−58.53	−63.45	−69.61	−67.90	−68.36	−74.76	−68.35	−67.87	−64.12
Rx2_130	−54.30	−63.97	−70.13	−68.42	−68.88	−75.28	−68.87	−68.39	−64.64
Rx2_140	−54.98	−53.36	−59.51	−57.81	−58.26	−64.66	−58.25	−57.78	−54.02
Rx2_150	−40.34	−48.39	−54.60	−52.89	−53.35	−59.75	−53.34	−52.86	−49.11
Rx2_160	−37.92	−35.65	−41.81	−40.10	−40.56	−46.96	−40.55	−40.07	−36.32
Rx2_170	−39.38	−31.34	−37.50	−35.79	−36.24	−42.65	−36.23	−35.76	−32.01
Rx2_180	−46.20	−35.01	−35.50	−39.44	−39.89	−46.30	−39.88	−39.41	−35.66
<b>RMSE</b>		7.3694	10.2147	8.5859	8.8307	13.4507	8.8252	8.5706	7.4062

When we examined the values of  $\mu$  and  $\varepsilon$  from literature, we took the average losses for position 1 with all rotations (due to single wall reflection) and the average losses for position 2 with all rotations (due to two reflections). It was found that when using the same values of  $\mu$  and  $\varepsilon$ , losses due to two reflections are 1.8 times of losses due to a single reflection. This suggests that multiple reflections are likely to be the dominant cause for such losses.

Simulated results for the ray reflected from two concrete walls are presented in Table 4. Values are taken from [29], Refs. [33] and [32] (a) give the best result while values taken from [35] give the worst results.

#### Case 2: Reflection from a wooden board for 210–250° rotations

The paths with the strongest RSS at the second location with rotations (210–250°) were reflected from the wooden board as shown in Figure 13. The ray is clearly not from the bore-sight as shown in this figure; therefore, the simulated values will be slightly different from those from the measurements.

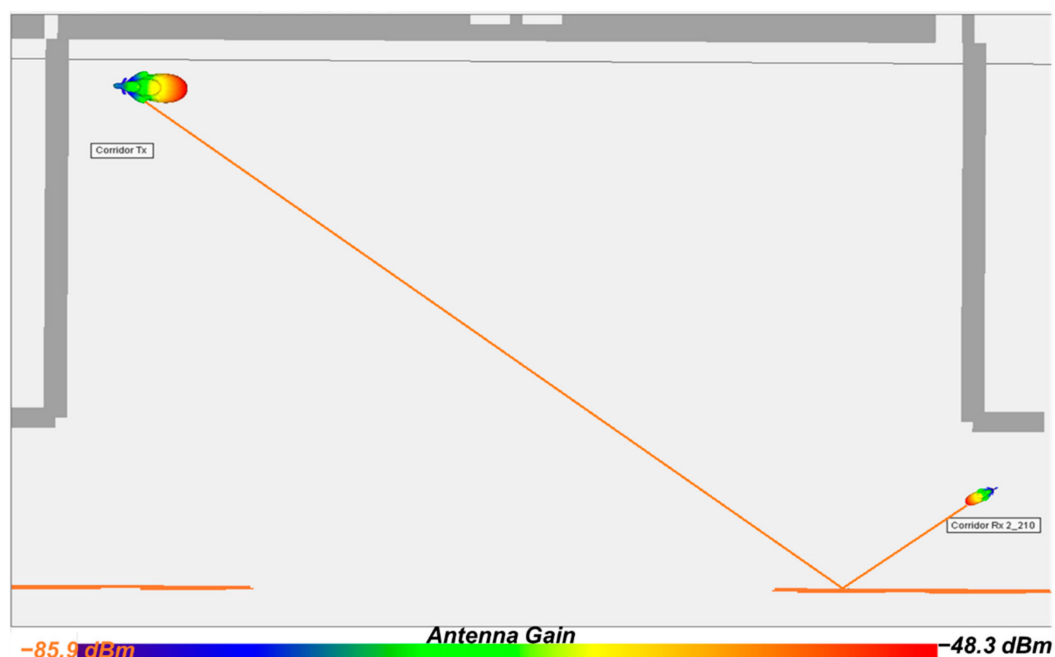


Figure 13. Reflection from the wooden wall (strongest paths for all Rx2 (210–250°)).

Figure 14 shows a performance comparison between measurements and simulations at Rx2 (receiver's antenna gain was set to 26 dB). The closest performance is obtained when using values from [35], while the worst performance is obtained when using values from [29] (b), where the mean difference between simulation results is around 5.26 dB. The RMSE between the best results and measurements is around 12.26 dB, which is a relatively high value.

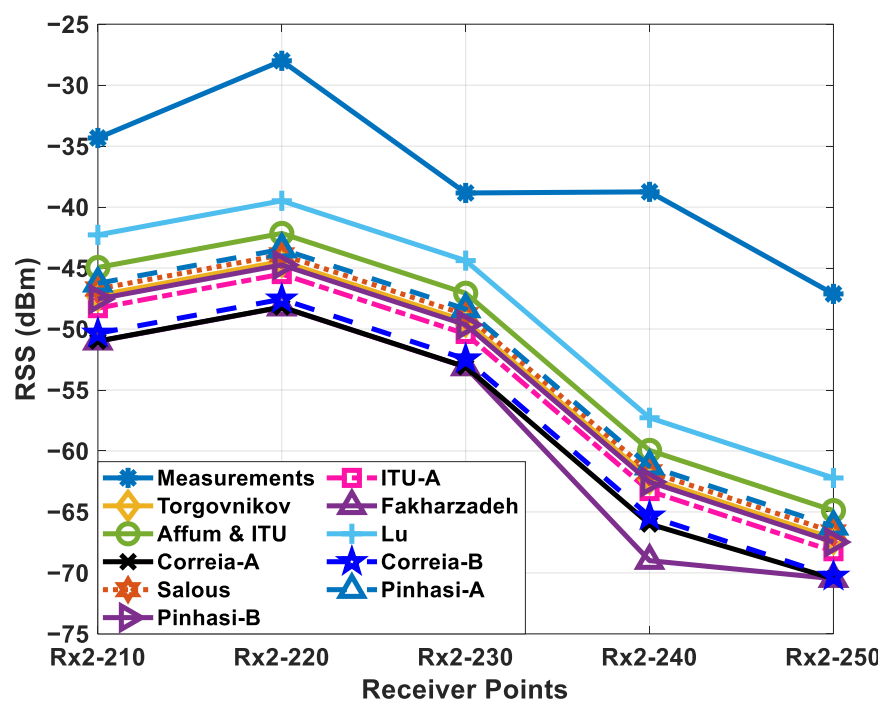
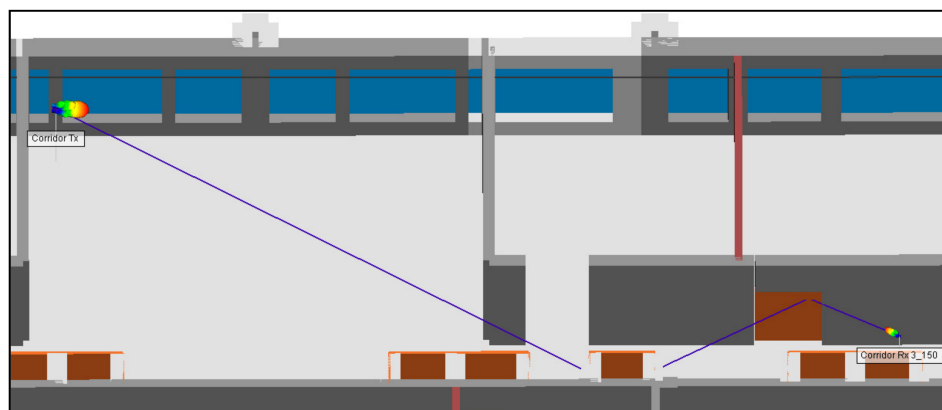


Figure 14. Performance comparison between references at Rx2 (210–250°).

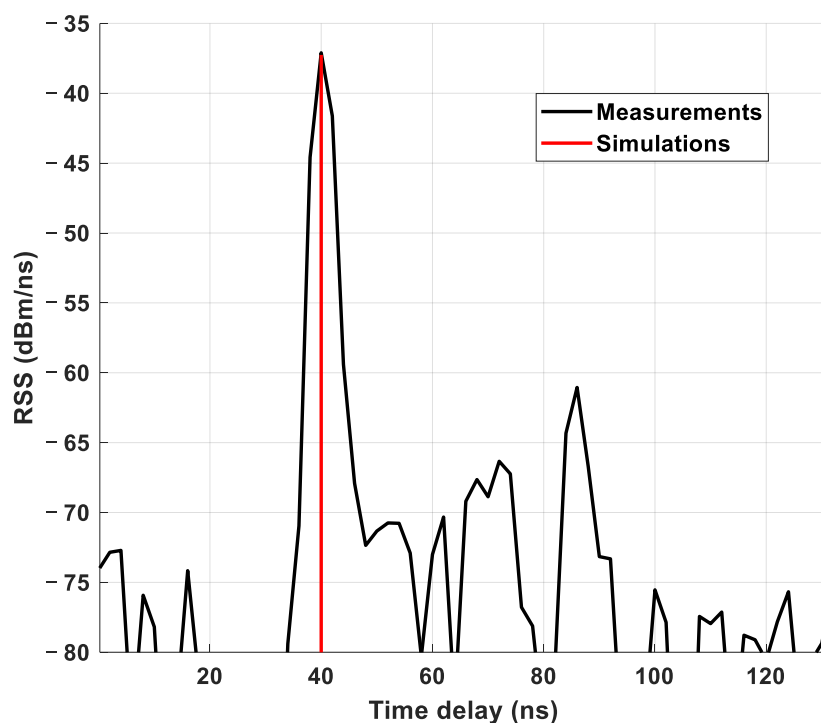
#### 4.2.3. Position 3: (Reflection on Two Wooden Surfaces)

Figure 15 presents the strongest path between the transmitter and the receiver at the third position with  $150^\circ$  and  $160^\circ$  rotations and a 24 dBi receiver antenna gain. As seen in this figure, the strongest ray is reflected from two wooden surfaces.



**Figure 15.** Reflection from two wooden surfaces strongest paths for all Rx3, RSS =  $-37.25$  dBm.

The PDP is presented in Figure 16. The RSS of the strongest path in the measurements is  $-37.11$  dBm while the simulation result is  $-37.25$  dBm and shows near-perfect agreement. However, another three measurements have an RSS bigger than  $-70$  dBm, where the Wireless InSite did not show; and the software overestimated the transmission losses and thus yielding pessimistic results.



**Figure 16.** PDP at Rx3\_150.

Table 5 presents a performance comparison between references from the literature and measurements at the receiver Position 3. As seen from this table, the effect of rotating 10 degrees resulted in the measured value being more than 14 dB. This clearly shows how sensitive and unpredictable the channel is. For all data taken from the literature, such a sudden change was not observed when changing the complex permittivity values.

**Table 5.** Performance comparison between references from literature and measurements at the third receiver position.

	Rotations	
	Rx3_150°	Rx3_160°
Measured	−37.11	−52.14
[32] (a)	−50.05	−49.03
[31]	−48.73	−47.72
[34]	−54.60	−53.60
[37] + [32] (a)	−44.70	−43.70
[35]	−37.25	−39.77
[36] (a)	−54.55	−53.54
[36] (b)	−56.93	−55.91
[38]	−47.70	−46.69
[29] (a)	−46.80	−45.79
[29] (b)	−48.94	−47.93

In general, best results are obtained for wooden surfaces, when complex permittivity values from reference [35] are used. In contrast, best results are obtained for concrete when relative permittivity values are within the range 11–13 as in [33] and [29], and conductivity values in the range 0.8967–0.988 as in [32] (a) and [29].

The obtained results suggest that the building material in references [33] and [32] (a) for concrete and in [35] for wood may be more similar to the building material in the examined environment compared to other references. Therefore, values in other references are not necessarily inaccurate and may be suitable for other environments. Results also show that WI can be used for channel propagation estimation at the 60 GHz band.

Wireless InSite software is sensitive to complex permittivity values, antenna pattern, dimensions of the environment and the exact locations of transmitters and receivers. As long as the user takes into account these factors, results can be considered as representative.

## 5. Conclusions

In this paper, the sensitivity of Wireless InSite results is explored when applied at different material properties from literature at 60 GHz. The study includes indoor LOS and NLOS propagation scenarios. It was found that WI is sensitive to changes in complex permittivity values, antenna dimensions, antenna pattern, and accuracy of the environment design. It was also observed that results integrity heavily depends on selecting the correct complex permittivity values from the literature. In short, the materials selected from the literature should be similar to those of the environment under study to have accurate results. Values of the same material found in other references are not necessarily inaccurate and they may be suitable for other environments. Generally speaking, WI is sensitive to input parameters and the environment design. The more accurate parameters and design, the better real-life propagation scenarios.

**Author Contributions:** Conceptualization, H.O.; methodology, H.O.; software, H.O. and W.M.; validation, O.O. and Y.D.; formal analysis, H.O., A.U., A.A. and W.M.; resources, A.U., A.A. and W.S.; writing—original draft preparation, H.O. and W.M.; writing—review and editing, H.O. and O.O.; visualization, W.S.; supervision, C.K.-Z. and R.A.-A.; project administration R.A.-A. All authors have read and agreed to the published version of the manuscript.

**Funding:** This work is partially supported by the innovation programme under grant agreement H2020-MSCA-ITN-2016 SECRET-722424 and the financial support from the UK Engineering and Physical Sciences Research Council (EPSRC) under grant EP/E022936/1.

**Data Availability Statement:** The data presented in this study are available on request from the corresponding author.

**Conflicts of Interest:** The authors declare no conflict of interest

## References

1. Nitsche, T.; Cordeiro, C.; Flores, A.B.; Knightly, E.W.; Perahia, E.; Widmer, J.C. IEEE 802.11 ad: Directional 60 GHz communication for multi-Gigabit-per-second Wi-Fi. *IEEE Commun. Mag.* **2014**, *52*, 132–141. [\[CrossRef\]](#)
2. Yilmaz, T.; Fadel, E.; Akan, O.B. Employing 60 GHz ISM Band for 5G Wireless Communications. In Proceedings of the 2014 IEEE International Black Sea Conference on Communications and Networking (BlackSeaCom), Chisinau, Moldova, 27–30 May 2014; IEEE: New York, NY, USA, 2014; pp. 77–82.
3. Roh, W.; Seol, J.-Y.; Park, J.; Lee, B.; Lee, J.; Kim, Y.; Cho, J.; Cheun, K.; Aryanfar, F. Millimeter-wave beamforming as an enabling technology for 5G cellular communications: Theoretical feasibility and prototype results. *IEEE Commun. Mag.* **2014**, *52*, 106–113. [\[CrossRef\]](#)
4. Cordeiro, C. The pursuit of tens of gigabits per second wireless systems [Industry Perspectives]. *IEEE Wirel. Commun.* **2013**, *20*, 3–5. [\[CrossRef\]](#)
5. Guo, N.; Qiu, R.C.; Mo, S.S.; Takahashi, K. 60-GHz millimeter-wave radio: Principle, technology, and new results. *EURASIP J. Wirel. Commun. Netw.* **2006**, *2007*, 68253. [\[CrossRef\]](#)
6. Liu, P.; Di Renzo, M.; Springer, A. Line-of-sight spatial modulation for indoor mmWave communication at 60 GHz. *IEEE Trans. Wirel. Commun.* **2016**, *15*, 7373–7389. [\[CrossRef\]](#)
7. Rappaport, T.S.; Heath, R.W., Jr.; Daniels, R.C.; Murdock, J.N. *Millimeter Wave Wireless Communications*; Pearson Education: New York, NY, USA, 2015; ISBN 0132172283.
8. Hansen, C.J. WiGiG: Multi-gigabit wireless communications in the 60 GHz band. *IEEE Wirel. Commun.* **2011**, *18*, 6–7. [\[CrossRef\]](#)
9. Saha, S.K.; Ghasempour, Y.; Haider, M.K.; Siddiqui, T.; De Melo, P.; Somanchi, N.; Zakrajsek, L.; Singh, A.; Shyamsunder, R.; Torres, O. X60: A programmable testbed for wideband 60 ghz wlans with phased arrays. *Comput. Commun.* **2019**, *133*, 77–88. [\[CrossRef\]](#)
10. Pang, J.; Maki, S.; Kawai, S.; Nagashima, N.; Seo, Y.; Dome, M.; Kato, H.; Katsuragi, M.; Kimura, K.; Kondo, S. A 50.1-Gb/s 60-GHz CMOS transceiver for IEEE 802.11 ay with calibration of LO feedthrough and I/Q imbalance. *IEEE J. Solid State Circuits* **2019**, *54*, 1375–1390. [\[CrossRef\]](#)
11. Ghasempour, Y.; da Silva, C.R.C.M.; Cordeiro, C.; Knightly, E.W. IEEE 802.11 ay: Next-generation 60 GHz communication for 100 Gb/s Wi-Fi. *IEEE Commun. Mag.* **2017**, *55*, 186–192. [\[CrossRef\]](#)
12. Wu, X.; Wang, C.-X.; Sun, J.; Huang, J.; Feng, R.; Yang, Y.; Ge, X. 60-GHz millimeter-wave channel measurements and modeling for indoor office environments. *IEEE Trans. Antennas Propag.* **2017**, *65*, 1912–1924. [\[CrossRef\]](#)
13. AlAbdullah, A.A.; Ali, N.; Obeidat, H.; Abd-Alhameed, R.A.; Jones, S. Indoor Millimetre-Wave Propagation Channel Simulations at 28, 39, 60 and 73 GHz for 5G Wireless Networks. In Proceedings of the 2017 Internet Technologies and Applications (ITA), North East Wales, UK, 12–15 September 2017; IEEE: New York, NY, USA, 2017; pp. 235–239.
14. Saha, S.K.; Vira, V.V.; Garg, A.; Koutsonikolas, D. A feasibility study of 60 GHz indoor WLANs. In Proceedings of the 2016 25th International Conference on Computer Communication and Networks (ICCCN), Waikoloa, HI, USA, 1–4 August 2016; IEEE: New York, NY, USA, 2016; pp. 1–9.
15. Saha, S.K.; Malleshappa, D.G.; Palamanda, A.; Vira, V.V.; Garg, A.; Koutsonikolas, D. 60 GHz indoor WLANs: Insights into performance and power consumption. *Wirel. Netw.* **2018**, *24*, 2427–2450. [\[CrossRef\]](#)
16. Salous, S.; Gao, Y. Wideband Measurements in Indoor and Outdoor Environments in the 30 GHz and 60 GHz Bands. In Proceedings of the 2016 10th European Conference on Antennas and Propagation (EuCAP), Davos, Switzerland, 10–15 April 2016; IEEE: New York, NY, USA, 2016; pp. 1–3.
17. Rangan, S.; Rappaport, T.S.; Erkip, E. Millimeter-wave cellular wireless networks: Potentials and challenges. *Proc. IEEE* **2014**, *102*, 366–385. [\[CrossRef\]](#)
18. Sulyman, A.I.; Seleem, H.; Alwarafy, A.; Humadi, K.M.; Alsanie, A. Effects of solar radio emissions on outdoor propagation path loss models at 60 GHz bands for access/backhaul links and D2D communications. *IEEE Trans. Antennas Propag.* **2017**, *65*, 6624–6635. [\[CrossRef\]](#)
19. Diakhate, C.A.L.; Conrat, J.-M.; Cousin, J.-C.; Sibille, A. Millimeter-Wave Outdoor-to-Indoor Channel Measurements at 3, 10, 17 and 60 GHz. In Proceedings of the 2017 11th European Conference on Antennas and Propagation (EuCAP), Paris, France, 19–24 March 2017; IEEE: New York, NY, USA, 2017; pp. 1798–1802.
20. Manan, W.; Obeidat, H.; Al-Abdullah, A.; Abd-Alhameed, R.; Hu, F. Indoor to indoor and indoor to outdoor millimeter wave propagation channel simulations at 26 Ghz, 28 Ghz and 60 Ghz for 5G mobile networks. *Int. J. Eng. Sci* **2018**, *7*, 8–18.
21. Obeidat, H.; Alabdullah, A.; Elkhazmi, E.; Suhaib, W.; Obeidat, O.; Alkhambashi, M.; Mosleh, M.; Ali, N.; Dama, Y.; Abidin, Z.; et al. Indoor environment propagation review. *Comput. Sci. Rev.* **2020**, *37*, 100272. [\[CrossRef\]](#)
22. Mededović, P.; Velečić, M.; Blagojević, Ž. Wireless insite software verification via analysis and comparison of simulation and measurement results. In Proceedings of the 2012 35th International Convention MIPRO, Opatija, Croatia, 21–25 May 2012; pp. 776–781.

23. Obeidat, H.A.; Obeidat, O.A.; Mosleh, M.F.; Abdullah, A.A.; Abd-Alhameed, R.A. Verifying Received Power Predictions of Wireless InSite Software in Indoor Environments at WLAN Frequencies. *Appl. Comput. Electromagn. Soc. J.* **2020**, *35*, 1119–1126. [\[CrossRef\]](#)
24. Dama, Y.A.S.; Abd-Alhameed, R.A.; Salazar-Quinonez, F.; Zhou, D.; Jones, S.M.R.; Gao, S. MIMO Indoor Propagation Prediction Using 3D Shoot-and-Bounce Ray (SBR) Tracing Technique for 2.4 GHz and 5 GHz. In Proceedings of the 5th European Conference on Antennas and Propagation (EUCAP), Rome, Italy, 11–15 April 2011; IEEE: New York, NY, USA, 2011; pp. 1655–1658.
25. Remcom. *Wireless InSite Reference Manual*, 3.1.0; Remcom: State College, PA, USA, 2017.
26. Balanis, C.A. *Antenna Theory: Analysis and Design*; John Wiley & Sons: Hoboken, NJ, USA, 2016; ISBN 1118642066.
27. Series, P. Effects of building materials and structures on radiowave propagation above about 100 MHz. *Recomm. ITU-R* **2015**, 2040–2041. Available online: [https://www.itu.int/dms\\_pubrec/itu-r/rec/p/R-REC-P.2040-1-201507-I!!PDF-E.pdf](https://www.itu.int/dms_pubrec/itu-r/rec/p/R-REC-P.2040-1-201507-I!!PDF-E.pdf) (accessed on 1 December 2020).
28. Correia, L.M.; Frances, P.O. Transmission and isolation of signals in buildings at 60 GHz. Proceedings of 6th International Symposium on Personal, Indoor and Mobile Radio Communications, Toronto, ON, Canada, 27–29 September 1995; Volume 3, p. 1031.
29. Pinhasi, Y.; Yahalom, A.; Petnev, S. Propagation of ultra wide-band signals in lossy dispersive media. In Proceedings of the 2008 IEEE International Conference on Microwaves, Communications, Antennas and Electronic Systems, Tel Aviv, Israel, 13–14 May 2008; pp. 1–10.
30. Stavrou, S.; Saunders, S.R. Review of Constitutive Parameters of Building Materials. In Proceedings of the Twelfth International Conference on Antennas and Propagation, 2003 (ICAP 2003), Exeter, UK, 31 March–3 April 2003; IET: London, UK, 2003; Volume 1, pp. 211–215.
31. Torgovnikov, G.I. *Dielectric Properties of Wood and Wood-Based Materials*; Springer: Berlin/Heidelberg, Germany, 1993.
32. Series, P. Propagation data and prediction methods for the planning of indoor radiocommunication systems and radio local area networks in the frequency range 900 MHz to 100 GHz. *Recomm. ITU-R* **2012**, 1237–1238. Available online: [https://www.itu.int/dms\\_pubrec/itu-r/rec/p/R-REC-P.1238-8-201507-S!!PDF-E.pdf](https://www.itu.int/dms_pubrec/itu-r/rec/p/R-REC-P.1238-8-201507-S!!PDF-E.pdf) (accessed on 1 December 2020).
33. Fares, M.; Fargier, Y.; Villain, G.; Derobert, X.; Lopes, S.P. Determining the permittivity profile inside reinforced concrete using capacitive probes. *NDT E Int.* **2016**, *79*, 150–161. [\[CrossRef\]](#)
34. Fakharzadeh, M.; Nezhad-Ahmadi, M.-R.; Biglarbegian, B.; Ahmadi-Shokouh, J.; Safavi-Naeini, S. CMOS phased array transceiver technology for 60 GHz wireless applications. *IEEE Trans. Antennas Propag.* **2010**, *58*, 1093–1104. [\[CrossRef\]](#)
35. Lu, J.; Steinbach, D.; Cabrol, P.; Pietraski, P.; Pragada, R.V. Propagation Characterization of An Office Building in the 60 GHz Band. In Proceedings of the 8th European Conference on Antennas and Propagation (EuCAP 2014), The Hague, The Netherlands, 6–11 April 2014; IEEE: New York, NY, USA, 2014; pp. 809–813.
36. Correia, L.M.; Frances, P.O. Transmission and isolation of signals in buildings at 60 GHz. In Proceedings of the 6th International Symposium on Personal, Indoor and Mobile Radio Communications, Helsinki, Finland, 13–16 September 2011; IEEE: New York, NY, USA, 1995; Volume 3, p. 1031.
37. Affum, E.; Tchao, E.T.; Diawuo, K.; Agyekum, K. Wideband Parameters Analysis and Validation for Indoor radio Channel at 60/70/80 GHz for Gigabit Wireless Communication employing Isotropic, Horn and Omni directional Antenna. *arXiv* **2013**, arXiv:1312.5109. [\[CrossRef\]](#)
38. Salous, S.; Degli Esposti, V.; Fuschini, F.; Thomae, R.S.; Mueller, R.; Dupleich, D.; Haneda, K.; Garcia-Pardo, J.-M.M.; Garcia, J.P.; Gaillot, D.P. Millimeter-Wave Propagation: Characterization and modeling toward fifth-generation systems. *[Wireless Corner]. IEEE Antennas Propag. Mag.* **2016**, *58*, 115–127. [\[CrossRef\]](#)